The role of high-mobility group box protein 1 in chronic cerebral hypoperfusion-induced vascular cognitive impairment animals

Amelia Nur Vidyanti
Taipei Medical University
Jia-Yu Hsieh
Taipei Medical University
Kun-Ju Lin
Chang Gung Memorial Hospital Linkou Branch
Yao-Ching Fang
Taipei Neuroscience Institute
Ismail Setyopranoto
Universitas Gadjah Mada Fakultas Kedokteran
Chaur-Jong Hu (chaurjongh@tmu.edu.tw)
Taipei Medical University https://orcid.org/0000-0002-4900-5967

Research

Keywords: vascular cognitive impairment, chronic cerebral hypoperfusion, bilateral common carotid artery occlusion, HMGB1, CRISPR/Cas9-KO plasmid

Posted Date: November 9th, 2019

DOI: https://doi.org/10.21203/rs.2.17046/v1

Abstract

Background: The molecular mechanisms of vascular cognitive impairment (VCI) are diverse and still in puzzle. VCI could be attributed to chronic cerebral hypoperfusion (CCH). CCH may cause a cascade of reactions involved in ischemia and neuro-inflammation which plays important roles in the pathophysiology of VCI. High-mobility group box protein 1 (HMGB1) is a non-histone protein that serves as a damage-associated molecular signal leading to cascades of inflammation. Increased level of HMGB1 has been established in the acute phase of CCH. However, the role of HMGB1 at the chronic phase of CCH remains elucidated. Methods: We performed modified bilateral common carotid artery occlusion (BCCAO) in C57BL/6 mice to induce CCH. We examined the cerebral blood flow (CBF) reduction by laser doppler flowmetry, the protein expression of HMGB1 and its pro-inflammatory cytokines (TNF-a, IL-1b, and IL-6) by western blotting and immunohistochemistry. The brain pathology was assessed by 7T-animal MRI and amyloid-b accumulation was assessed by amyloid-PET scanning. We further evaluated the effect of HMGB1 suppression by injecting CRISPR/Cas9 knock-out plasmid intra-hippocampus bilaterally. Results: There were reduction of CBF up to 50% which persisted three months after CCH. The modified-BCCAO animals developed significant cognitive decline. The 7T-MRI image showed hippocampal atrophy, although the amyloid-PET showed no significant amyloid-beta accumulation. Increased protein levels of HMGB1, TNF-a and IL-1b were found three months after BCCAO. HMGB1 suppression by CRISPR/Cas9 knock-out plasmid restored the CBF, IL-1B, TNF-alpha, IL-6, and attenuated hippocampal atrophy and cognitive decline. Conclusion: HMGB1 plays a pivotal role in the pathophysiology of the animal model of CCH and it might be a candidate as therapeutic targets of VCI.

Background

Vascular cognitive impairment (VCI) after Alzheimer's disease is the second leading cause of dementia worldwide. It includes clinical spectrums of cognitive decline ranging from mild vascular cognitive impairment to vascular dementia. One major cause of cognitive decline in VCI is chronic cerebral hypoperfusion (CCH) (1). CCH may develop in many conditions with impairment of cerebral vascular system such as hypotension, extreme hypertension, diabetes mellitus, atherosclerosis, smoking and carotid or cerebral artery stenosis (2). Animal models of CCH showed that persistent decrease of cerebral blood flow was followed by production of reactive oxygen species and proinflammatory cytokines. Eventually it may damage neuronal cells and lead to neurodegeneration (3-6).

Cerebral hypoperfusion exerts its neuronal damage by triggering at least two sequences of excitotoxicity (7, 8). First is related to abrupt depletion of adenosine triphosphate (ATP) from sudden decrease of cerebral blood flow (CBF). This ischemic condition causes neuronal necrosis in acute stage. Second, when the CBF gradually restores but still in moderate CBF reduction, the ATP level is still low and this condition may result in neuronal apoptosis. However, the neuronal death after CCH is not solely a typical necrosis or apoptosis. Instead, it involved a complexity of molecular and biochemical mechanisms along with the apoptosis-necrosis continuum (9, 10).

Necrotic neurons further release a high mobility group box protein 1 (HMGB1). HMGB1 is a non-histone protein which serves as a crucial cytokine produced in response to infection, injury and inflammation. It is normally located in the nucleus (11). HMGB1 can be either actively secreted by inflammatory cells or passively released by necrotic or died cells. HMGB1 when it is located extracellularly will subsequently induce the cascade of inflammation by binding to toll-like receptor 4 (TLR4) or *receptor* for advanced glycation end products (RAGE) (12).

The role of HMGB1 has been widely established in acute stroke and traumatic brain injury as it is responsible for the neuronal damage and the worsening symptoms. There are also several studies about HMGB1 induced chronic inflammation and neurodegeneration in Alzheimer's disease (AD), amyotrophic lateral sclerosis, Parkinson disease and multiple sclerosis. Previous study revealed that HMGB1 could impair neurit outgrowth in mice model of AD and led to cognitive decline (13). In human study, serum HMGB1 increased significantly in AD patients and correlated well with the level of amyloid-b (14). The HMGB1 is also believed to cause disruption of blood-brain-barrier integrity (15).

Nonetheless, the detailed mechanisms of HMGB1 in mediating cognitive decline at the chronic phase after CCH have not been established yet. Previous experimental model of CCH only demonstrated that the administration of anti-HMGB1 neutralizing antibody at acute stage of ischemia could reserve hippocampal neuronal death and improve cognitive impairment (16). Although the positive effect of that antibody remains even in 12 weeks, the persistence of high HMGB1 at the chronic phase of CCH has not been investigated. In addition, it is still not clear whether the suppression of HMGB1 in the chronic phase would also be beneficial. In this study, for the first time, we used modified bilateral common carotid artery occlusion to induce CCH in mice and suppressed the HMGB1 level by CRISPR/Cas9 knock-out plasmid during the chronic stage. Hence, we aimed to figure out the role of HMGB1 in the chronic stage of CCH and to explore its potential application on vascular cognitive impairment.

Methods

Animals and study design

Male C57bl/6j mice (16-week-old, weighing 25 to 35 grams, Bio-Lasco Taiwan Co., Ltd) were used for all the experiments. They were placed under controlled temperature (22 ± 1°C) and humidity (55 ± 10%) with a 12 h light/dark cycle (lights on at 07:00 h). Food and water were given as libitum to all mice throughout the experiments. Animal care and experimental procedures in this study had been approved and were in accordance with the guidelines for the Care and Use of Laboratory Animals from Ethics Committee of Taipei Medical University.

The mice groups were divided into two parts: part one was before HMGB1 CRISPR/Cas9 KO plasmid injection, and part two was after the injection. For part one, the mice were randomly grouped as sham-control (n=12) and BCCAO (n=12). For part two, the mice were randomly grouped as sham-CRISPR control, sham-CRISPR HMGB1 KO, BCCAO-CRISPR control, and BCCAO-CRIPSR HMGB1 KO. Each group in part two had six mice (Fig. 1). This study followed the ARRIVE guidelines.

Model establishment of CCH by modified bilateral common carotid artery occlusion (BCCAO) surgery

The modified-BCCAO was performed by ligating both the common carotid artery (CCA) but with some modification from the previous procedure (17, 18). Due to mice were dead soon after both of the CCA were ligated simultaneously, hence one of the CCA was ligated transiently for 30 minutes. The animals were anesthetized with isoflurane 2%. Cerebral blood flow (CBF) was measured while doing the surgery. A sagital midline incision (~1 cm length) was performed to expose the parietal skull. The skin was carefully dissected and a fiberoptic probe of laser doppler flowmetry (LDF) was put directly to the skull 2 mm caudal and 5 mm lateral from bregma to measure the CBF. A cervical midline neck incision (~1 cm length) was made. Both salivatory glands were carefully separated and mobilized to visualize the underlying common carotid artery (CCA). Both CCA were carefully separated from the respective vagal nerves and accompanying veins without harming these structures. A tight, double 5-0 silk suture loop (proximal & distal) was made around right CCA. Re-measured the CBF, there must be a reduction of CBF by 80-90% from the baseline. Finally, we closed the wound by suturing.

One week later, the procedure was repeated for left CCA. The steps were similar except there was transient ligation of left CCA. A small polyethylene tubing (diameter 0,58 mm) was inserted in between the left CCA and the silk sutures. This tubing was used as a splinting of the left CCA in order to avoid damaging of the arterial walls when the sutures were tightened. Left CCA was occluded for 30 minutes by tightening the silk sutures. Then, we re-measured the CBF and there must be a reduction of CBF by 80-90% from the baseline. After 30 minutes, released the ligation of left CCA and removed the polyethylene tubing. After the whole procedure, mice were put in a heating pad for 30 minutes while waiting them awake. After awaking, they were put back into their cages. The procedure of sham-surgery was similar with BCCAO excluding the ligation of both CCA.

Injection of HMGB1 CRISPR/Cas9-KO plasmid

The HMG-1 Crispr/Cas9 KO plasmid (sc-400735) and HMG-1 HDR plasmid (sc-400735-HDR) were purchased from Santa Cruz Biotechnology, Inc. HMG-1 Crispr/Cas9 KO plasmid consisted of a pool of three plasmids each encoding the Cas9 nuclease and a HMGB-1-specific 20 nt guide RNA (gRNA) designed for maximum knockout efficiency. gRNA sequences were derived from the GeCKO (v2) library and direct the Cas9 protein to induce a site-specific double strand break (DSB) in the genomic DNA. HMG-1 HDR plasmid consisted of a pool of 2-3 plasmids, each containing a homology-directed DNA repair (HDR) template corresponding to the cut sites generated by the HMG-1 Crispr/Cas9 KO plasmid. Each HDR template contained two 800 bp homology arm designed to specifically bind to the genomic DNA surrounding the corresponding Cas9-induced double-strand DNA break site.

We injected HMG-1 Crispr/Cas9 KO plasmid and HMG-1 HDR plasmid mixed with jetSI^{TM} 10mM transfection reagent according to manufacturer's recommendations. A total volume of 4 mL of the mixture was injected into each hippocampus (anteroposterior [AP] – 2 mm, mediolateral [ML] – 1.5 mm, and dorsoventral [DV] – 2 mm related to bregma), at a rate of 0.4 mL/min by a 26-gauge Hamilton syringe under isoflurane anesthesia. For CRISPR control group, we injected a vehicle with the same volume and procedure. The injection was conducted at 1 month after BCCAO/sham surgery. Two months after injection, the mice had an MRI examination to evaluate the brain pathology and hippocampal atrophy as well as a novel object recognition (NOR) test.

Novel object recognition (NOR)

Mice tend to interact more with a novel object than with a familiar one. This tendency has been used by behavioral pharmacologists and neuroscientists to study learning and memory. A popular protocol for such research is the object recognition task (19). The procedure consisted of three phases: habituation phase, sample phase, and test phase. We perform this procedure with modifications (20). During habituation phase, each mouse was allowed to explore the field in the absence of objects for 10 min for two consecutive days in order to make them become familiar with the field. On the third day during the sample phase, two objects were placed symmetrically onto the arena. The mice were placed at the mid-point of the wall opposite the sample objects with its body parallel to the side walls and its nose pointing away from the objects, allowed to freely explore for 5 min. Time spent exploring the objects was recorded. During the test phase, one of the two objects used in sample phase was randomly replaced by a novel one, then the mice were re-introduced to the arena for 5 min exploration after a 4-hours delay. Between each mouse, any feces were cleared, the arena and objects were cleaned with 70% ethyl alcohol. The video tracking system was used to collect behavioral performances automatically. The time spent exploring both the novel and the familiar objects was recorded (TN, TF). Object discrimination was evaluated by the recognition index (RI): RI = TN/(TN + TF).

Motor function test

Beam walking test: Further subtle motor coordination and balance were assessed using a modified balance beam (beam walking) test. This procedure was based on modified protocol describe in Luong et al (2011) (21). The beam apparatus consisted of 1-meter beams with a round-rough surface of 12 mm (or 6 mm width) resting 50 cm above the table top on two poles. A black box was placed at the end of the beam as the finish point. Food was placed in the black box to attract the mouse to the finish point. A lamp (with 60-watt light bulb) was used to shine light above the start point and serves as an aversive stimulus. The time to cross the center 80 cm was measured manually: one at 0 cm that started a timer and one at 80 cm that stopped the timer. A video camera was set on a tripod to record the performance. This test took place over 3 consecutive days: 2 days of training and 1 day of testing. On training days,

each mouse crossed the 12 mm (or 6 mm) beam 3 times. On the test day, time to cross each beam were recorded. Two successful trials in which the mouse did not stall on the beam were averaged. Video recordings could be used for finer analysis of slipping and other observable motor deficits.

Rotarod: Briefly, gross motor control was measured using the rotarod (IITC Life Science, CA, USA). This procedure was based on the protocol described in Tung et al. (2014) with some modification (22). For this test, each mouse was placed on a cylindrical dowel (69.5 mm in diameter) raised 27 cm above the floor of a landing platform. Mice were placed on the dowels for 5 min to allow them to acclimatize to the test apparatus. Once initiated, the cylindrical dowels began rotating and accelerated from 5 rpm to a final speed of 44 rpm over 60 s. During this time, mice were required to walk in a forward direction on the rotating dowels for as long as possible. When the mice were no longer able to walk on the rotating dowels, they fell onto the landing platform below. This triggered the end of the trial for an animal and the measurements of time to fall (TTF) were collected. Passive rotations where mice clung to, and consequently rotated with the dowel were also used to define the end of the trial. Mice were then returned to their cages with access to food and water for 10 min. This procedure took 3 days; day 1 and 2 were for training (each day consisted of 2-3 trials), and day 3 was for testing (consisted of 2 trials). The trials from testing day was used for analysis.

MRI (7T-aMRI)

MRI experiments to monitor the brain condition (e.g. atrophy and white matter lesion) after BCCAO were performed with a 7T horizontal MRI scanner (Bruker PharmaScan 70/16, USA), with a 7T/40cm magnet (Biospect Bruker console) and a surface coil. The mice were initially anesthetized with 3.0% isoflurane (Escain, Mylan Japan, Tokyo, Japan) and then with 1.5% to 2.0% isoflurane and 1:5 oxygen/room-air mixture during the MRI experiments. Rectal temperature was continuously monitored using an optical thermometer (FOT-M, FISO, Quebec, QC, Canada) and maintained at 37.0 °C ± 0.5 °C using a heating pad (Temperature control unit, Rapid Biomedical), and warm air was provided by a homemade automatic heating system based on an electric temperature controller (E5CN, Omron, Kyoto, Japan) throughout the MRI experiments. During MRI scanning, the mice laid in a prone position on an MRI-compatible cradle and were held in place by handmade ear bars. The first imaging slices were carefully set at the rhinal fissure, with reference to a mouse brain atlas. The modality of MRI performed was T2-weighted spin echo.

Trans-axial T2-weighted images were acquired using rapid acquisition with a relaxation enhancement (RARE) sequence as follows: TR/TE = 2500/33 ms, slice number/thickness = 16/0.75 mm, matrix = 256 × 256, FOV = 16 × 16 mm^2, average = 8, RARE factor = 8, flip angel = 90, scan time = 10 min 40s. Volumes of the hippocampus and lateral ventricles were measured using MRIcron software (NITRC 2016).

Amyloid-PET scanning

For amyloid-PET scanning, the mice were anesthetized with isoflurane (1.5%, delivered via a mask at 3.5 L/min in oxygen) and received bolus injection of 18.5 MBq/0.2 cc of ^{18}F-AV45 (Eli Lily, IN, USA) via the tail vein with a catheter. Following placement in the scanner (Inveon, Siemens Medical Solutions, Germany), a 10 min transmission scan was obtained using a rotating ^{57}Co point source, followed by a single frame emission recording for the interval 40–60 min post-injection. The PET image reconstruction procedure consisted of a 3-dimensional ordered subset expectation maximization (OSEM) with four iterations and 12 subsets followed by a maximum a posteriori (MAP) algorithm. Scatter and attenuation correction were performed and a decay correction for ^{18}F was applied. With a zoom factor of 1.0 and a 128 x 128 x 159 matrix, a final voxel dimension of 0.78 x 0.78 x 0.80 mm was obtained. The image analysis was performed by using PMOD (PMOD version 3.7, Technologies Ltd, Switzerland). A manual rigid-body re-alignment of individual ^{18}F-AV45 images on a ^{18}F-AV45 template was performed using the PMOD fusion tool. The normalized PET images were co-registered to a magnetic resonance imaging brain template for region of interest delineation. Using the predefined mice brain MRI template of PMOD and manual ROI of frontal lobe and hippocampus fused with co-registered AV-45 PET/CT image, the AV-45 signal in the region of interests were determined, respectively.

Western Blot

Mice were anesthetized with isoflurane 2% then decapitated. Brain were collected from the skull and separated into 3 regions in each hemisphere: cortex, hippocampus, and striatum. Since hippocampal tissue was very tiny, we combined right and left hippocampus for western blot experiment. Protein samples of each region were extracted in the following manner. Individual tissue samples were homogenized in lysis buffer (50 mmol/L Tris, pH 7.4, 1 mmol/L EDTA, 1 mmol/L phenylmethylsulfonyl fluoride, 4 lg/mL aprotinin and leupeptin, 1% sodium dodecyl sulfate), protease inhibitor cocktail solution and phosphatase inhibitor cocktail solution (GenDEPOT, Barker, TX, USA). The homogenates were then centrifuged at 13.400 × g for 30 minutes at 4°C, and the supernatants were harvested, snap-frozen, and stored at −80°C. The protein concentration of the supernatants was determined using the bradford assay. Equal amounts of protein (20 μg) were then separated via SDS-PAGE and transferred to a PVDF membrane, which were subsequently incubated in a primary antibody (Ab) against HMGB1 (mouse monoclonal antibody, 1:1000, GeneTex, USA), IL-1β (rabbit polyclonal antibody, 1:1000, GeneTex, USA), TNF-a (rabbit polyclonal antibody, 1:1000, GeneTex, USA) and IL-6 (rabbit polyclonal antibody, 1:1000, GeneTex, USA). Following incubation in the primary Ab, the membranes were incubated in horseradish peroxidase (HRP)-conjugated secondary Ab (Cell Signaling, MA, USA) and then detected using an ECL system (Thermo Scientific, MA, USA) with a UVP Biospectrum AC system (Fisher Scientific, USA). Densitometry is performed for specific markers normalized to b-actin (1:1000, clone C4, Millipore Corporation, USA) using Image J (v1.37) software.

Immunostaining

On 3 months after the BCCAO or sham surgery, the mice were anesthetized and intracardially perfused with phosphate-buffered saline (PBS), followed by 4% paraformaldehyde. The brains were removed, post-fixed 4 hours in 4% paraformaldehyde at 4 °C and stored in 30% sucrose in 0.1 M PBS (pH 7.4). Serial coronal-cryopreserved sections cut at 30 μm thickness that spanned from the anterior of the corpus callosum (bregma 0.26 mm) to the anterior of the hippocampus (bregma 0.94 mm) (adjusted according to the mouse brain atlas) (23) using a cryostat. The slides then were permeabilized with 0.5% Triton X-100 in PBS for 2 hours. After being blocked with BlockPRO (VISUAL PROTEIN) at room temperature for 1 h, the brain slides were incubated with the following primary antibodies: mouse monoclonal anti-HMGB1 antibody (1:100, GeneTex, USA), rabbit polyclonal anti-TNF-α (1:100, GeneTex, USA), rabbit polyclonal anti-IL-6 (1:100, GeneTex, USA) and rabbit polyclonal anti-IL-1β (1:100, GeneTex, USA) at 4 °C overnight. The brain slides were then incubated with secondary antibodies conjugated to Alexa 488 (1:1000; Thermo Fisher Scientific, MA, USA) or Alexa 594 (1:500; Thermo Fisher Scientific, MA, USA) for 2-h at RT. Brain sections were then washed and counterstained with 2 μg/mL DAPI (Life Technologies) for 20 min at RT. Fluorescence images were obtained using a Tissue FAXS system (TISSUE GNOSTICS) with a ×25 objective lens. For the triple stained, tissue slides were incubated with primary antibodies: mouse monoclonal anti-HMGB1 antibody (1:100, GeneTex, USA) and rabbit polyclonal anti-NeuN (1:300, Cell Signaling, USA). The images were obtained by using Confocal Microscope with ×63 oil objective lens. All images were taken at 1024 × 1024-pixel resolution.

Statistical analysis

One-way ANOVA followed by Sidak post-hoc test was used to analyze western blot results, IF, and CBF measurement. NOR results were analyzed by using two-way ANOVA. Student unpaired t-test was used to analyze motor function MRI results. All analyses were performed by using GraphPad Prism 7 software (GraphPad Software, La Jolla, CA). The statistically significance was considered when the p value was less than 0.05.

Results

Survival rate and CBF values

All procedures of modified-BCCAO were accomplished within 15 minutes, except for waiting time of 30 minutes to transiently ligate the left common carotid artery. After 3 months of BCCAO surgery, all mice had survived.

In the control group (sham-surgery), the mean CBF at 1 month and 3 months after the sham surgery did not change much from baseline. In contrast, the CBF values decreased significantly in the BCCAO group.

The CBF values in right cerebral cortex decreased to 57.5% ± 13.6% and 73.4% ± 15.5% (mean ± SD) in left cerebral cortex at 1 month after surgery (Fig. 2a). At 3 months after surgery, the CBF values remained low in BCCAO mice. They decreased to 58.4% ± 3.3% and 69.9% ± 4.4% in the right side and left side, respectively (Fig. 2a). This CBF changes in BCCAO group were significantly different compared with sham group (sham, n=6; BCCAO, n=6).

CCH induced hippocampal atrophy and memory decline, but did not cause behavioral alterations in motor coordination

To investigate the effects of CCH on motor coordination, we performed rotarod test and beam-balance walking test at 3 months after surgery (Fig. 2b, c). We found that BCCAO did not alter motor coordination, indicating there was no injury in cortical or subcortical lesion.

To study whether CCH impair memory function, Novel Object Recognition (NOR) test was conducted. This test can be used to assess non-spatial working memory which describes some parts of hippocampus function and its relationship with perirhinal cortex (24) as well as frontal subcortical circuits (25). The BCCAO mice showed worse performance to recognize the familiar object than sham mice at 1 and 3 months after surgery (Fig. 2d, e; $F(2, 28) = 8.815$, $p<0.01$). Compare with sham-mice, BCCAO mice spent less time exploring the novel object when tested at 3 hours after training phase. Hence, the results of recognition index (RI) were <50%, indicates a short-term memory deficit in BCCAO mice due to impairment of memory retention for novel object or more preference to the familiar object (26, 27) .

Hippocampal atrophy is associated with cognitive decline in dementia cases (28-30). To delineate this, hippocampal volumes were measured in sham and BCCAO mice at 1 and 3 months after surgery using T2-weighted image. Hippocampal atrophy was found during the time course after the surgery in BCCAO mice, but not in sham mice. BCCAO mice showed significant reduction of total hippocampal volume than sham mice at 1 and 3 months after surgery (Fig. 2f, g: $p<0.05$).

CCH is expected to cause amyloid-beta (Ab) accumulation particularly in Alzheimer's disease (31-34). We also investigated whether CCH induced by BCCAO could develop Ab accumulation at 3 months after surgery by doing amyloid-PET scanning. However, we found no Ab accumulation in BCCAO mice (Fig. 3).

CCH increased the expression of HMGB1 at 3 months

CCH will induce neuroinflammation (30, 35). However, there are plenty cascades of inflammation involved in CCH. We found that CCH induced by BCCAO altered the level of HMGB1 in cortex, striatum, and hippocampus at 3 months (Fig. 4). At 1 month after BCCAO surgery, we did not find any alteration of HMGB1 expression either in cortex, striatum or hippocampus (data not shown).

The expression of HMGB1 at chronic phase of CCH was further confirmed by immunostaining (Fig. 5). We found consistent findings that HMGB1 was expressed more in BCCAO mice. The pro-inflammatory cytokines such as TNF-a, and IL-1b were also up-regulated. In addition, IL-6 was likely to increase in BCCAO mice compare to sham. All of them serve as the downstream signaling pathway of HMGB1.

The source of increased level of HMGB1 was from neuronal cells, mostly concentrated in the cytosol and some were released extracellularly. This was revealed by the triple-staining of HMGB1/NeuN/DAPI as shown in Fig. 6.

Administration of CRISPR/Cas9-KO of HMGB1 in BCCAO mice decreases the expression of HMGB1, restores CBF, attenuates hippocampal atrophy, and improves cognitive decline

To further delineate the role of HMGB1 at the chronic phase of CCH, we injected the HMGB1 CRISPR/Cas9 knock-out (KO) plasmid for suppressing the HMGB1 expression. The injection was done at 1 month after CCH. Two months after injection, the BCCAO HMGB1-KO mice showed a restored CBF, decreased level of HMGB1 from their brain tissue, attenuated the hippocampal atrophy, and improved the cognitive decline (Fig. 7). The decreased expression of HMGB1 was further confirmed by immunostaining as it also demonstrated decreased expression of pro-inflammatory cytokines (TNF-a, IL-1b, and IL-6) (Fig. 8).

Discussion

This is the first study to explore the role of HMGB1 at the chronic phase of chronic cerebral hypoperfusion (CCH) in a mouse model of VCI induced by modified-BCCAO. This is also the first study to use HMG-1 CRISPR/Cas9 KO plasmid to suppress HMGB1 in CCH. We found increased HMGB1 in 3 months after CCH together with reduced cerebral blood flow (CBF) ratio from baseline, hippocampal neuronal loss or atrophy and declined memory function. The administration of HMG-1 CRISPR/Cas9 KO plasmid at 1 month after surgery could reverse those consequences of CCH (Fig. 9).

Animal models establishment of CCH caused by common carotid artery occlusion have been verified by previous study using bilateral common carotid artery (BCCAO) in rats (36, 37), bilateral carotid artery stenosis (BCAS) in mice (5, 30, 38, 39) or gerbil (40), and unilateral common carotid artery occlusion (UCCAO) in mice (4, 41). The rat model is the most widely used among the other models of CCH. However, it has limitation as causing damage in the visual pathway by occluding the ophthalmic artery thus may influence the behavioral assessment (42). It also has quite high mortality rates, ranging between 7%-25% depends on the strains used (43). The mice BCAS model also has higher mortality rate with microcoils of 0.16 mm in diameter (75% mortality rate) and variably mortality rates with microcoils of 0.18 mm in

diameter (15-19%), 0.20 mm (17%), and 0.22 mm (13%) (44). The mice UCCAO model has no mortality but only induces mild short-term memory loss due to very mild reduction of CBF (42). The present study demonstrated that CCH induced by modified-BCCAO surgery caused moderate hypoperfusion at 1 and 3 months after the surgery. There was no mortality of animals. The CBF ratio was persistently reduced to 50-70% from baseline even after 3 months. Previous study used quantitative measurement by laser speckle imaging revealed that in bilateral carotid artery stenosis (BCAS) model, the CBF decreased to 62.9% at 2 hours after surgery and gradually restored to 81.7% at 1 month, 83.2% at 2 months, and 85.0% at 3 months(5). Another model of VCI, UCCAO (unilateral common carotid artery occlusion), has been showed that decreased of CBF measured by laser Doppler flowmetry to about 20-37% at 28 days after surgery (4, 28). In this present study we show, for the first time to our knowledge, that the CBF ratio remains low at 3 months after surgery (5, 6, 45, 46). The results in the present study might be caused by the procedure of BCCAO consists of 2 steps which allows less risk of death and persistently moderate reduction of CBF until 3 months after surgery.

CCH model in the present study significantly impairs the non-spatial memory function as showed by the lower recognition index (less than 0.5) in the NOR test. The similar findings were also found in other studies of CCH whether BCAS, UCCAO, or BCCAO was used in rats. NOR test could demonstrate the essential function of hippocampus (especially the dorsal part) and perirhinal cortex (47, 48). These two structures are responsible for non-spatial and short-term memory function (24, 25). This result was further supported by hippocampal atrophy found from MRI image. Hippocampus is the most vulnerable region after global cerebral ischemia or CCH, especially CA1 neurons. Therefore, hippocampal atrophy could be found as the consequence of neuronal loss after CCH (6, 49-51). We did not observe any motoric disturbance at 3 months after surgery, indicates that CCH does not alter motor cortex or other structures associated with motoric function. This is in agreement with prior studies (4, 33, 52).

In the present study, we did not find any Ab accumulation. It suggests that the process of CCH only might not adequate to induce Ab accumulation in C57BL/6 mice. It needs other factors than CCH to initiate Ab deposition. Previous studies reported that Ab accumulation found in AD transgenic mice (at 5 months of age) after 1-month CCH induced by BCAS (33, 53). In another study, 3 months old of AD transgenic mouse demonstrated Ab overproduction, decreased α-secretase activity and expression, as well as increased β-secretase activity and expression after 1-month CCH induced by UCCAO (54). Nevertheless, a study using rat with BCCAO showed that CCH could promote Ab pathogenesis by activating β/γ-secretases (55); and a study using C57BL/6 mice reported that CCH increased Ab levels and enhanced β/γ-secretase levels after 6 months of BCAS (31). The latest findings suggest that CCH in wild type mice could possibly induce Ab accumulation or promote Ab pathogenesis only if CCH was applied in longer time period. However, this hypothesis still needs further investigation.

Previous study has demonstrated the increased HMGB1 release at the acute phase of hypoperfusion induced subsequently persistent neuroinflammation (16). However, in the present study we found remarkable increased of HMGB1 at the chronic phase of CCH, in terms of 3 months. In the present study, the increased HMGB1 were found in cytosols of neuronal cells which could then be released

extracellularly. The increased level of HMGB1 in the cytosol might be a response of dying cells or surrounding cell death due to hypoxia and ischemia caused by CCH which eventually leads to neuronal loss (3, 56, 57). It is speculated that increased HMGB1 level at this chronic phase should not be released from necrotic neurons. It is possibly released by apoptotic neurons since apoptosis is the main cause of neuronal death found at the chronic phase of CCH (6, 58). In contrary, necrosis is the main findings at the acute phase of CCH (6). Since the role of HMGB1 in chronic stage of CCH has never been explored, the increased HMGB1 level in the present study could be a novel finding to support the contribution of HMGB1 at the chronic phase of CCH. It could also serve as another piece of evidence that HMGB1 is possibly released by apoptotic neurons under CCH.

Once HMGB1 is released extracellularly, it will bind to TLR2, TLR4, or RAGE receptors, then activating NF-KB pathway to initiate the production of pro-inflammatory cytokines such as IL-1b, IL-6, TNF-a (11, 12). As confirmed by our findings, TNF-a and IL-1b levels were found higher in BCCAO compared to sham mice at 3 months after CCH. However, we did not find any increased level of TLR2/4, RAGE, or protein involved in NF-KB signaling pathway (data not shown). These findings implicated that HMGB1 triggered the downstream inflammation pathway without changes of levels of its receptors. That might highlight the important role of HMGB1 in the pathophysiology of VCI induced by CCH. The administration of HMGB1 CRISPR/Cas9 KO plasmid could suppress the HMGB1 levels as well as the pro-inflammatory cytokines (TNF-a, IL-1b, and IL-6) and restore CBF. Moreover, the knock-out of HMGB1 successfully attenuated hippocampal atrophy and improved cognitive impairment at the chronic phase of CCH. The therapeutic effect of HMGB1 KO plasmid by CRIPRS/Cas9 system demonstrated in this study shows that the suppression of HMGB1 resulted in not only with the inhibition of neuro-inflammation but also increase of CBF. Nevertheless, the restoration of CBF after HMGB1 suppression is contrary to previous studies (16, 59, 60). Noteworthy that previous studies investigated the effect of HMGB1 neutralization on CBF changes at the acute phase of ischemia. Therefore, the findings from previous studies might have a different scenario from the present study.

The mechanisms related to CBF restoration after HMGB1 suppression is unknown. It could probably involve the vascular smooth muscle cells (VSMC) and cerebrovascular endothelial cells (CVEC) migration and remodeling (61, 62). Both VSMC and CVEC affected by nitric oxide (NO) are very important to maintain the vascular tone and regulate CBF. Another possible mechanism could be related to iNOS or eNOS/NO signaling pathway. Previous studies showed that inhibition of HMGB1 could reduce the expression of iNOS (63, 64). As well known, inducible nitric oxide synthase (iNOS) could lead to NO overproduction which triggers peroxidative process and released of free radical species (65, 66). It could induce endothelial dysfunction caused by impairment of eNOS/NO signaling pathway which subsequently decrease the CBF (65). However, the direct effects of HMGB1 on eNOS/NO signaling pathway which is the most important mediator for vessel dilatation are still unclear which should be further investigated to delineate the exact mechanisms.

The present study has some limitations. First, we only investigated the effects of HMGB1 suppression at one single dose and one period of time, in terms of 2 months after CRISPR injection. This is a concept-

proving study, the effects of this suppression by different doses, as well as given for different periods of time should be warrant if clinical application is considered in the future. Second, we did not investigate the role of HMGB1 in glial cells. Previous studies showed that HMGB1 could also be released rapidly after cerebral ischemia by astrocytes, or as late as 1 week after ischemia by microglia (19, 67). Moreover, it has been established that HMGB1 would activate glial cells once it released by the dying neurons (12, 64). Therefore, investigating the role of HMGB1 in glial cells after CCH might be beneficial in the future studies. Next, the underlying mechanisms by which HMGB1 exerts its pro-inflammatory action after CCH is not totally clear in this study. Previous studies have proved that HMGB1 would bind to TLR2/TLR4 and/or RAGE which did not change in this study to initiate downstream inflammatory pathway (68, 69). The molecular mechanisms of how HMGB1 affect CBF in this CCH model also needs further investigations. Moreover, we only performed diffusion tensor imaging (DTI) and failed to detect white matter tract lesions (data not shown). The previous studies demonstrated that CCH induced white matter lesions (5, 30, 41, 70-72), Investigations with the histological examination and/or electrophysiological measurement may be considered for the future study.

Conclusion

This study demonstrated for the first time that HMGB1 significantly contributes to cognitive impairment at the chronic phase of CCH, in part by modulating pro-inflammatory cytokines (TNF-a, IL-1b, and IL-6) and CBF changes. The administration of HMG-1 CRISPR/Cas9 KO plasmid could reverse the cognitive impairment and restore the CBF. Thus, the suppression of HMGB1 expression might be a promising therapeutic target for vascular cognitive impairment due to CCH.

Abbreviations

VCI: vascular cognitive impairment; CCH: chronic cerebral hypoperfusion; HMGB1: high-mobility group box protein 1; BCCAO: bilateral common carotid artery occlusion; CBF: cerebral blood flow; TNF-a: tumor necrosis factor-a; IL-1b: interleukin-1b; IL-6: interleukin-6; 7T-MRI: 7 Tesla-magnetic resonance imaging; PET: positron emission tomography; CRISPR/Cas9: clustered regularly interspaced short palindromic repeats/CRISPR-associated protein 9; KO: knock-out; ATP: adenosine tri-phosphate; TLR4: toll-like receptor 4; RAGE: receptor for advanced glycation end products; AD: Alzheimer's disease; CCA: common carotid artery; NOR: novel object recognition; Ab: amyloid-b: ANOVA: analysis of variance; VSMC: vascular smooth muscle cell; CVEC: cerebrovascular endothelial cell; NO: nitric oxide; DTI: diffusion tensor imaging.

Declarations

Acknowledgments

We thank PET-scan imaging facilities at Linkou Chang-Gung Memorial Hospital for providing the amyloid-PET scanning; and the technical staffs at Small Animal-based Magnetic Resonance Imaging Service,

Taipei Medical University for their technological assistance.

Authors' Contributions

ANV and CJH conceived and designed the study; ANV and HJY performed the experiments and analyzed the data; KJL performed PET scan imaging and analyzed the data imaging; ANV and CJH wrote the manuscript; YCF, IS and CJH contributed in critically reviewing the manuscript.

Funding

This study was supported by Taiwan Ministry of Science and Technology (MOST 106-2314-B-038-038-MY2).

Availability of data and materials

The datasets used and/or analyzed in the current study are available from the corresponding author on reasonable request.

Ethics approval and consent to participate

All experiments were performed following the guidelines from the Care and Use of Laboratory Animals and approved by the Ethics Committee of Taipei Medical University (Approval numbers: LAC-2016-0434). All efforts were made to minimize the suffering of the animals and reduce the number of animals used.

Consent for publication

Not applicable

Competing interests

The author(s) declared that they have no competing interests with respect to the research, authorship, and/or publication of this article.

References

1. Dichgans M, Leys D. Vascular Cognitive Impairment. Circ Res. 2017;120(3):573-91.
2. Hu X, De Silva TM, Chen J, Faraci FM. Cerebral vascular disease and neurovascular injury in ischemic stroke. Circulation research. 2017;120(3):449-71.
3. Duncombe J, Kitamura A, Hase Y, Ihara M, Kalaria RN, Horsburgh K. Chronic cerebral hypoperfusion: a key mechanism leading to vascular cognitive impairment and dementia. Closing the translational gap between rodent models and human vascular cognitive impairment and dementia. Clinical Science. 2017;131(19):2451-68.
4. Zhao Y, Gu J-h, Dai C-l, Liu Q, Iqbal K, Liu F, et al. Chronic cerebral hypoperfusion causes decrease of O-GlcNAcylation, hyperphosphorylation of tau and behavioral deficits in mice. Frontiers in aging neuroscience. 2014;6:10.
5. Shibata M, Ohtani R, Ihara M, Tomimoto H. White matter lesions and glial activation in a novel mouse model of chronic cerebral hypoperfusion. Stroke. 2004;35(11):2598-603.
6. Farkas E, Luiten PG, Bari F. Permanent, bilateral common carotid artery occlusion in the rat: a model for chronic cerebral hypoperfusion-related neurodegenerative diseases. Brain research reviews. 2007;54(1):162-80.
7. Thong-Asa W, Tilokskulchai K. Neuronal damage of the dorsal hippocampus induced by long-term right common carotid artery occlusion in rats. Iranian journal of basic medical sciences. 2014;17(3):220.
8. Arundine M, Tymianski M. Molecular mechanisms of calcium-dependent neurodegeneration in excitotoxicity. Cell calcium. 2003;34(4-5):325-37.
9. Martin LJ, Al-Abdulla NA, Brambrink AM, Kirsch JR, Sieber FE, Portera-Cailliau C. Neurodegeneration in excitotoxicity, global cerebral ischemia, and target deprivation: a perspective on the contributions of apoptosis and necrosis. Brain research bulletin. 1998;46(4):281-309.
10. Dong Y-F, Kataoka K, Toyama K, Sueta D, Koibuchi N, Yamamoto E, et al. Attenuation of brain damage and cognitive impairment by direct renin inhibition in mice with chronic cerebral hypoperfusion. Hypertension. 2011;58(4):635-42.
11. Tang D, Kang R, Zeh III HJ, Lotze MT. High-mobility group box 1, oxidative stress, and disease. Antioxidants & redox signaling. 2011;14(7):1315-35.
12. Lotze MT, Tracey KJ. High-mobility group box 1 protein (HMGB1): nuclear weapon in the immune arsenal. Nature Reviews Immunology. 2005;5(4):331.
13. De Souza A, Westra J, Limburg P, Bijl M, Kallenberg C. HMGB1 in vascular diseases: its role in vascular inflammation and atherosclerosis. Autoimmunity reviews. 2012;11(12):909-17.
14. Fujita K, Motoki K, Tagawa K, Chen X, Hama H, Nakajima K, et al. HMGB1, a pathogenic molecule that induces neurite degeneration via TLR4-MARCKS, is a potential therapeutic target for Alzheimer's disease. Scientific reports. 2016;6:31895.
15. Festoff BW, Sajja RK, van Dreden P, Cucullo L. HMGB1 and thrombin mediate the blood-brain barrier dysfunction acting as biomarkers of neuroinflammation and progression to neurodegeneration in Alzheimer's disease. Journal of neuroinflammation. 2016;13(1):194.

16. Hei Y, Chen R, Yi X, Long Q, Gao D, Liu W. HMGB1 neutralization attenuates hippocampal neuronal death and cognitive impairment in rats with chronic cerebral hypoperfusion via suppressing inflammatory responses and oxidative stress. Neuroscience. 2018;383:150-9.
17. Speetzen LJ, Endres M, Kunz A. Bilateral common carotid artery occlusion as an adequate preconditioning stimulus to induce early ischemic tolerance to focal cerebral ischemia. JoVE (Journal of Visualized Experiments). 2013(75):e4387.
18. Song J, Nan D, He Q, Yang L, Guo H. Astrocyte activation and capillary remodeling in modified bilateral common carotid artery occlusion mice. Microcirculation. 2017;24(6):e12366.
19. Kim J-B, Choi JS, Yu Y-M, Nam K, Piao C-S, Kim S-W, et al. HMGB1, a novel cytokine-like mediator linking acute neuronal death and delayed neuroinflammation in the postischemic brain. Journal of Neuroscience. 2006;26(24):6413-21.
20. Wang M, Iliff JJ, Liao Y, Chen MJ, Shinseki MS, Venkataraman A, et al. Cognitive deficits and delayed neuronal loss in a mouse model of multiple microinfarcts. Journal of Neuroscience. 2012;32(50):17948-60.
21. Luong TN, Carlisle HJ, Southwell A, Patterson PH. Assessment of motor balance and coordination in mice using the balance beam. JoVE (Journal of Visualized Experiments). 2011(49):e2376.
22. Tung VW, Burton TJ, Dababneh E, Quail SL, Camp AJ. Behavioral assessment of the aging mouse vestibular system. JoVE (Journal of Visualized Experiments). 2014(89):e51605.
23. Franklin KB, Paxinos G. The mouse brain in stereotaxic coordinates: Academic press New York:; 2008.
24. Manns JR, Eichenbaum H. A cognitive map for object memory in the hippocampus. Learning & Memory. 2009;16(10):616-24.
25. Driscoll I, Hamilton DA, Petropoulos H, Yeo RA, Brooks WM, Baumgartner RN, et al. The aging hippocampus: cognitive, biochemical and structural findings. Cerebral cortex. 2003;13(12):1344-51.
26. Antunes M, Biala G. The novel object recognition memory: neurobiology, test procedure, and its modifications. Cognitive processing. 2012;13(2):93-110.
27. Denninger JK, Smith BM, Kirby ED. Novel Object Recognition and Object Location Behavioral Testing in Mice on a Budget. J Vis Exp. 2018(141).
28. Mueller SG, Schuff N, Yaffe K, Madison C, Miller B, Weiner MW. Hippocampal atrophy patterns in mild cognitive impairment and Alzheimer's disease. Human brain mapping. 2010;31(9):1339-47.
29. Shang J, Yamashita T, Zhai Y, Nakano Y, Morihara R, Li X, et al. Acceleration of NLRP3 inflammasome by chronic cerebral hypoperfusion in Alzheimer’s disease model mouse. Neuroscience research. 2019;143:61-70.
30. Ihara M, Tomimoto H. Lessons from a mouse model characterizing features of vascular cognitive impairment with white matter changes. Journal of aging research. 2011;2011.
31. Wang L, Du Y, Wang K, Xu G, Luo S, He G. Chronic cerebral hypoperfusion induces memory deficits and facilitates Aβ generation in C57BL/6J mice. Experimental neurology. 2016;283:353-64.

32. Ashok A, Rai NK, Raza W, Pandey R, Bandyopadhyay S. Chronic cerebral hypoperfusion-induced impairment of Aβ clearance requires HB-EGF-dependent sequential activation of HIF1α and MMP9. Neurobiology of disease. 2016;95:179-93.
33. Salvadores N, Searcy JL, Holland PR, Horsburgh K. Chronic cerebral hypoperfusion alters amyloid-β peptide pools leading to cerebral amyloid angiopathy, microinfarcts and haemorrhages in Tg-SwDI mice. Clinical science. 2017;131(16):2109-23.
34. Bannai T, Iwata A, Mano T, Ohtomo R, Ohtomo G, Hashimoto T, et al. CHRONIC CEREBRAL HYPOPERFUSION INCREASES AMYLOID PLAQUES BY ACCELERATING AMYLOID BETA AGGREGATION IN APP/PS1 TRANSGENIC MICE. Alzheimer's & Dementia: The Journal of the Alzheimer's Association. 2018;14(7):P693-P4.
35. Du S-Q, Wang X-R, Xiao L-Y, Tu J-F, Zhu W, He T, et al. Molecular mechanisms of vascular dementia: what can be learned from animal models of chronic cerebral hypoperfusion? Molecular neurobiology. 2017;54(5):3670-82.
36. Wakita H, Tomimoto H, Akiguchi I, Kimura J. Glial activation and white matter changes in the rat brain induced by chronic cerebral hypoperfusion: an immunohistochemical study. Acta neuropathologica. 1994;87(5):484-92.
37. Sarti C, Pantoni L, Bartolini L, Inzitari D. Persistent impairment of gait performances and working memory after bilateral common carotid artery occlusion in the adult Wistar rat. Behavioural brain research. 2002;136(1):13-20.
38. Shibata M, Yamasaki N, Miyakawa T, Kalaria RN, Fujita Y, Ohtani R, et al. Selective impairment of working memory in a mouse model of chronic cerebral hypoperfusion. Stroke. 2007;38(10):2826-32.
39. Coltman R, Spain A, Tsenkina Y, Fowler JH, Smith J, Scullion G, et al. Selective white matter pathology induces a specific impairment in spatial working memory. Neurobiology of aging. 2011;32(12):2324. e7-. e12.
40. Kudo T, Tada K, Takeda M, Nishimura T. Learning impairment and microtubule-associated protein 2 decrease in gerbils under chronic cerebral hypoperfusion. Stroke. 1990;21(8):1205-9.
41. Yoshizaki K, Adachi K, Kataoka S, Watanabe A, Tabira T, Takahashi K, et al. Chronic cerebral hypoperfusion induced by right unilateral common carotid artery occlusion causes delayed white matter lesions and cognitive impairment in adult mice. Experimental neurology. 2008;210(2):585-91.
42. Jiwa NS, Garrard P, Hainsworth AH. Experimental models of vascular dementia and vascular cognitive impairment: a systematic review. J Neurochem. 2010;115(4):814-28.
43. Kim S-K, Cho K-O, Kim SY. White matter damage and hippocampal neurodegeneration induced by permanent bilateral occlusion of common carotid artery in the rat: comparison between wistar and sprague-dawley strain. The Korean Journal of Physiology & Pharmacology. 2008;12(3):89-94.
44. Ihara M, Taguchi A, Maki T, Washida K, Tomimoto H. A mouse model of chronic cerebral hypoperfusion characterizing features of vascular cognitive impairment. Cerebral Angiogenesis: Springer; 2014. p. 95-102.

45. Hattori Y, Enmi J-i, Iguchi S, Saito S, Yamamoto Y, Nagatsuka K, et al. Substantial reduction of parenchymal cerebral blood flow in mice with bilateral common carotid artery stenosis. Scientific reports. 2016;6:32179.
46. Neto CJBF, Paganelli RA, Benetoli A, Lima KCM, Milani H. Permanent, 3-stage, 4-vessel occlusion as a model of chronic and progressive brain hypoperfusion in rats: a neurohistological and behavioral analysis. Behavioural brain research. 2005;160(2):312-22.
47. Cohen SJ, Munchow AH, Rios LM, Zhang G, Ásgeirsdóttir HN, Stackman Jr RW. The rodent hippocampus is essential for nonspatial object memory. Current Biology. 2013;23(17):1685-90.
48. Kinnavane L, Amin E, Olarte-Sánchez CM, Aggleton JP. Detecting and discriminating novel objects: The impact of perirhinal cortex disconnection on hippocampal activity patterns. Hippocampus. 2016;26(11):1393-413.
49. Yang G, Kitagawa K, Matsushita K, Mabuchi T, Yagita Y, Yanagihara T, et al. C57BL/6 strain is most susceptible to cerebral ischemia following bilateral common carotid occlusion among seven mouse strains: selective neuronal death in the murine transient forebrain ischemia. Brain research. 1997;752(1-2):209-18.
50. Wahul AB, Joshi PC, Kumar A, Chakravarty S. Transient global cerebral ischemia differentially affects cortex, striatum and hippocampus in Bilateral Common Carotid Arterial occlusion (BCCAo) mouse model. Journal of chemical neuroanatomy. 2018;92:1-15.
51. Somredngan S, Thong-asa W. Neurological Changes in Vulnerable Brain Areas of Chronic Cerebral Hypoperfusion Mice. Annals of neurosciences. 2017;24(4):233-42.
52. Gooch J, Wilcock DM. Animal models of vascular cognitive impairment and dementia (VCID). Cellular and molecular neurobiology. 2016;36(2):233-9.
53. Kitaguchi H, Tomimoto H, Ihara M, Shibata M, Uemura K, Kalaria RN, et al. Chronic cerebral hypoperfusion accelerates amyloid β deposition in APPSwInd transgenic mice. Brain research. 2009;1294:202-10.
54. Yang H, Hou T, Wang W, Luo Y, Yan F, Jia J. The effect of chronic cerebral hypoperfusion on amyloid-β metabolism in a transgenic mouse model of Alzheimer's disease (PS1V97L). Journal of Alzheimer's Disease. 2018;62(4):1609-21.
55. Cai Z, Liu Z, Xiao M, Wang C, Tian F. Chronic Cerebral Hypoperfusion Promotes Amyloid-Beta Pathogenesis via Activating β/γ-Secretases. Neurochem Res. 2017;42(12):3446-55.
56. Miyamoto O, Auer R. Hypoxia, hyperoxia, ischemia, and brain necrosis. Neurology. 2000;54(2):362-.
57. Andersson U, Yang H, Harris H, editors. High-mobility group box 1 protein (HMGB1) operates as an alarmin outside as well as inside cells. Seminars in immunology; 2018: Elsevier.
58. Bennett SA, Tenniswood M, Chen J-H, Davidson CM, Keyes MT, Fortin T, et al. Chronic cerebral hypoperfusion elicits neuronal apoptosis and behavioral impairment. Neuroreport. 1998;9(1):161-6.
59. Liu K, Mori S, Takahashi HK, Tomono Y, Wake H, Kanke T, et al. Anti-high mobility group box 1 monoclonal antibody ameliorates brain infarction induced by transient ischemia in rats. The FASEB Journal. 2007;21(14):3904-16.

60. Takizawa T, Shibata M, Kayama Y, Shimizu T, Toriumi H, Ebine T, et al. High-mobility group box 1 is an important mediator of microglial activation induced by cortical spreading depression. Journal of Cerebral Blood Flow & Metabolism. 2017;37(3):890-901.
61. Yang H, Wang H, Czura CJ, Tracey KJ. The cytokine activity of HMGB1. Journal of leukocyte biology. 2005;78(1):1-8.
62. Wang L, Zhang Z, Liang L, Wu Y, Zhong J, Sun X. Anti-high mobility group box-1 antibody attenuated vascular smooth muscle cell phenotypic switching and vascular remodelling after subarachnoid haemorrhage in rats. Neuroscience letters. 2019:134338.
63. Kim JB, Lim CM, Yu YM, Lee JK. Induction and subcellular localization of high-mobility group box–1 (HMGB1) in the postischemic rat brain. Journal of neuroscience research. 2008;86(5):1125-31.
64. Muhammad S, Barakat W, Stoyanov S, Murikinati S, Yang H, Tracey KJ, et al. The HMGB1 receptor RAGE mediates ischemic brain damage. Journal of Neuroscience. 2008;28(46):12023-31.
65. Gliozzi M, Scicchitano M, Bosco F, Musolino V, Carresi C, Scarano F, et al. Modulation of Nitric Oxide Synthases by Oxidized LDLs: Role in Vascular Inflammation and Atherosclerosis Development. International journal of molecular sciences. 2019;20(13):3294.
66. Wang F, Cao Y, Ma L, Pei H, Rausch WD, Li H. Dysfunction of cerebrovascular endothelial cells: prelude to vascular dementia. Frontiers in aging neuroscience. 2018;10:376.
67. Hayakawa K, Mishima K, Nozako M, Hazekawa M, Mishima S, Fujioka M, et al. Delayed treatment with minocycline ameliorates neurologic impairment through activated microglia expressing a high-mobility group box1–inhibiting mechanism. Stroke. 2008;39(3):951-8.
68. Kim JH, Ko PW, Lee HW, Jeong JY, Lee MG, Kim JH, et al. Astrocyte-derived lipocalin-2 mediates hippocampal damage and cognitive deficits in experimental models of vascular dementia. Glia. 2017;65(9):1471-90.
69. Yang W, Li J, Shang Y, Zhao L, Wang M, Shi J, et al. HMGB1-TLR4 axis plays a regulatory role in the pathogenesis of mesial temporal lobe epilepsy in immature rat model and children via the p38MAPK signaling pathway. Neurochemical research. 2017;42(4):1179-90.
70. Choi B-R, Kim D-H, Back DB, Kang CH, Moon W-J, Han J-S, et al. Characterization of white matter injury in a rat model of chronic cerebral hypoperfusion. Stroke. 2016;47(2):542-7.
71. Wakita H, Tomimoto H, Akiguchi I, Matsuo A, Lin J-X, Ihara M, et al. Axonal damage and demyelination in the white matter after chronic cerebral hypoperfusion in the rat. Brain research. 2002;924(1):63-70.
72. Wang X, Lin F, Gao Y, Lei H. Bilateral common carotid artery occlusion induced brain lesions in rats: A longitudinal diffusion tensor imaging study. Magnetic resonance imaging. 2015;33(5):551-8.

Figures

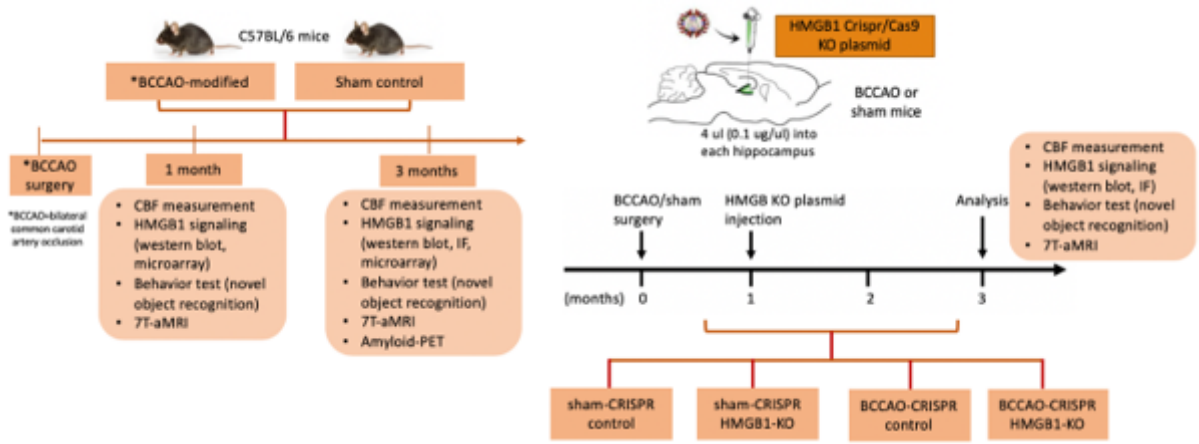

Figure 1

Schematic description of experimental design

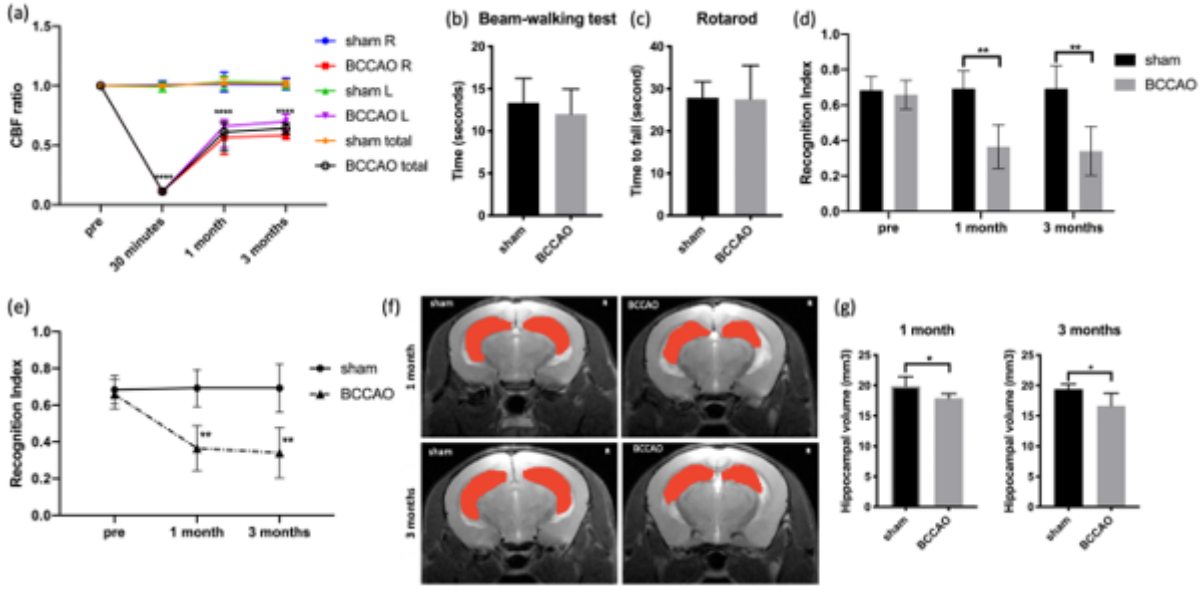

Figure 2

CCH induced CBF changes (a), memory decline (d, e), and hippocampal atrophy (f, g), but did not alter motor coordination (b, c) (*p<0.05; **p<0.01; ****p<0.0001)

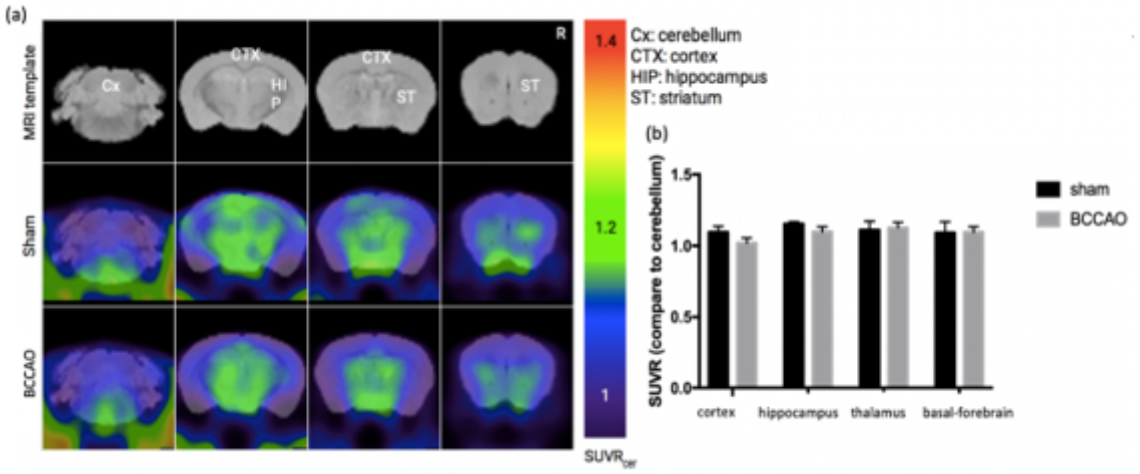

Figure 3

CCH induced by modified-BCCAO did not cause amyloid-beta accumulation after 3 months; a. Amyloid-PET scan image, b. Quantification data of Aβ accumulation were not different between sham and BCCAO mice in some brain regions

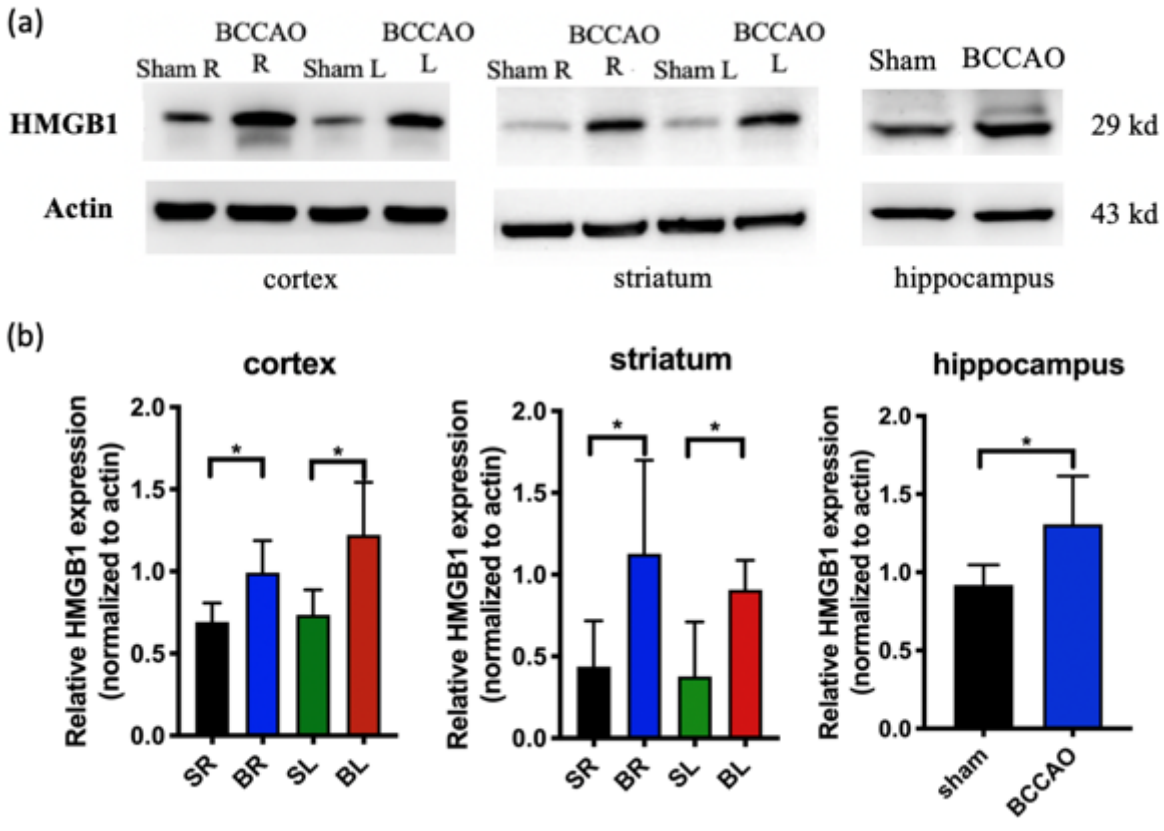

Figure 4

Increased HMGB1 in the cortex, striatum and hippocampus at 3 months after CCH; (a) Western blot results of HMGB1 in cortex, striatum, and hippocampus (R=right, L=left); (b) Quantification results of

HMGB1 relative protein in cortex, striatum, and hippocampus (SR=sham-right side, BR=BCCAO-right side, SL=sham-left side, BL=BCCAO-left side). (*p<0.05)

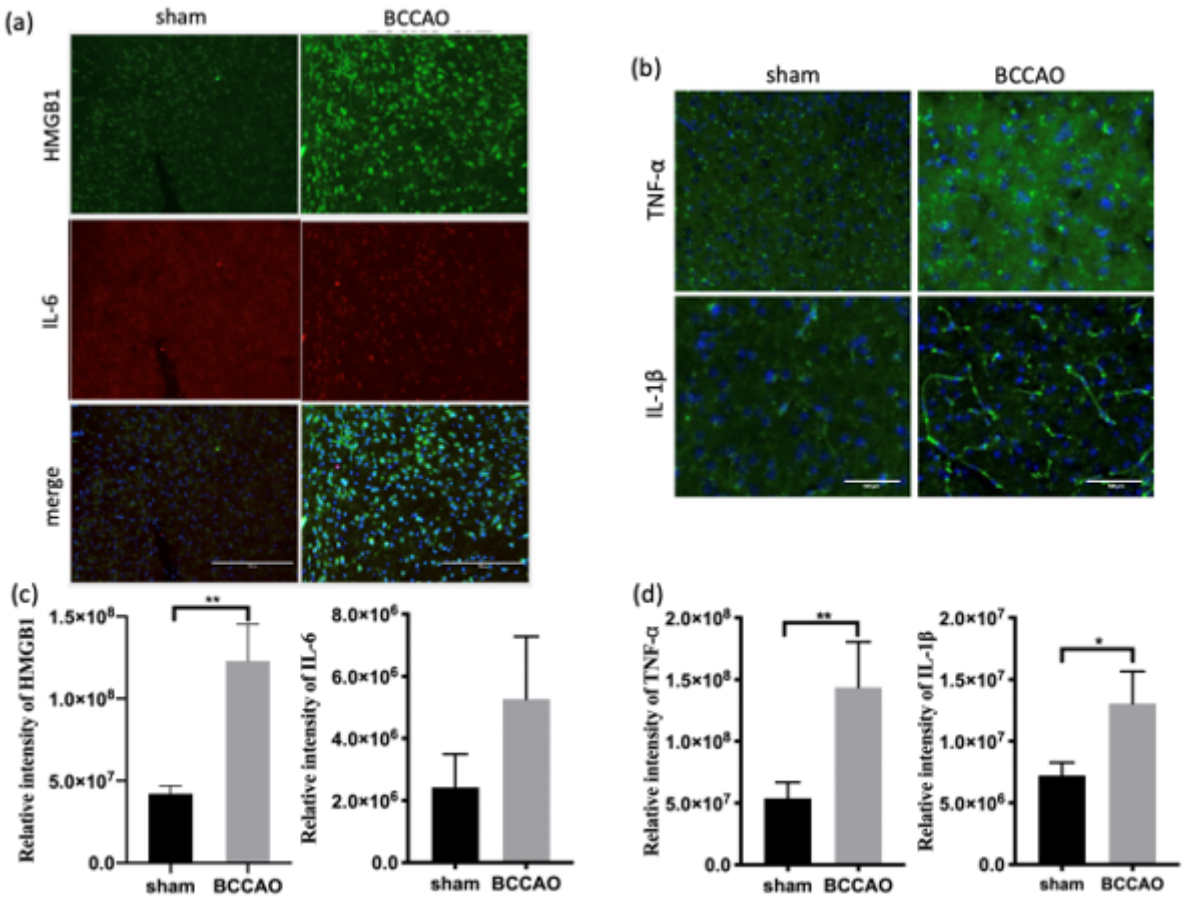

Figure 5

Increased expression of HMGB1, TNF-α, and IL-1β in cortex of CCH mice showed by immunofluorescence data (*p<0.05; **p<0.01); scale bar=100 μm

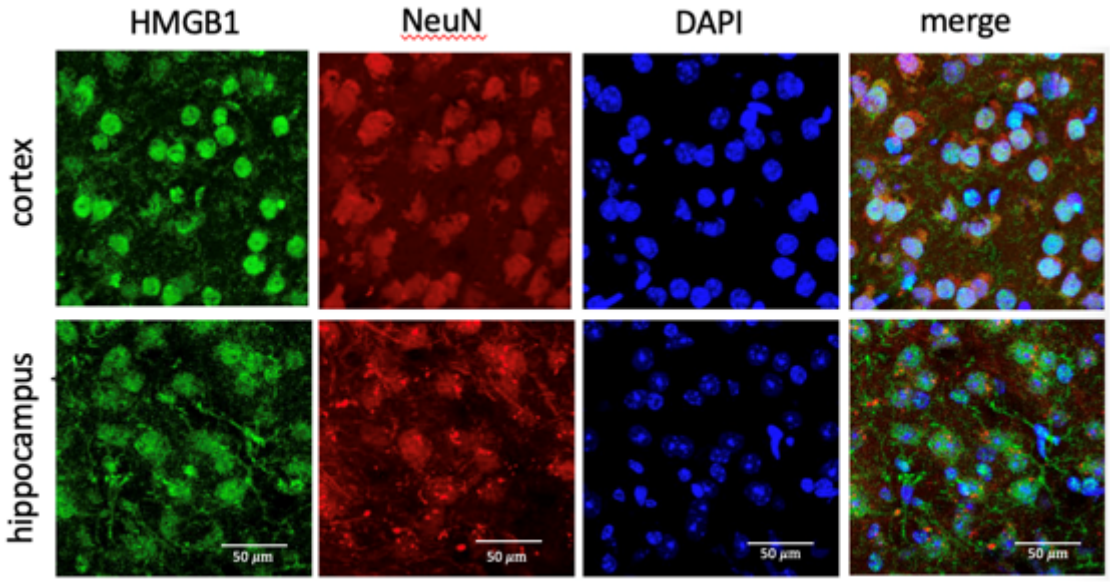

Figure 6

The triple-staining of HMGB1 with NeuN and DAPI from cortex and hippocampus of CCH mice. The source of increased HMGB1 were from neuronal cells, mainly located in the cytosols, and some were released extracellularly; scale bar= 50□m

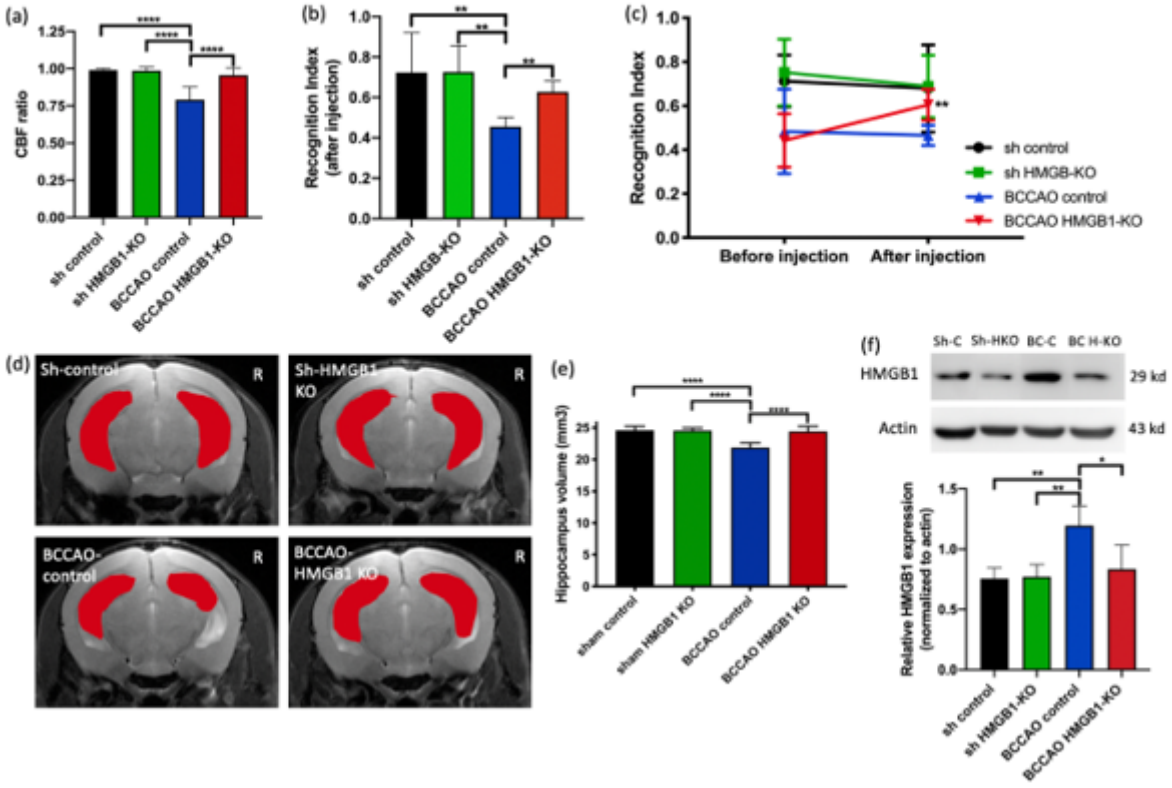

Figure 7

After injection of HMG-1 CRISPR/Cas9 KO plasmid, BCCAO HMGB1-KO mice showed a decrease of HMGB1 expression (f), recovered of CBF ratio (a), improvement of cognitive performance (b, c), and restored of hippocampal atrophy (d, e) (*p<0.05; **p<0.01; ***p<0.001)

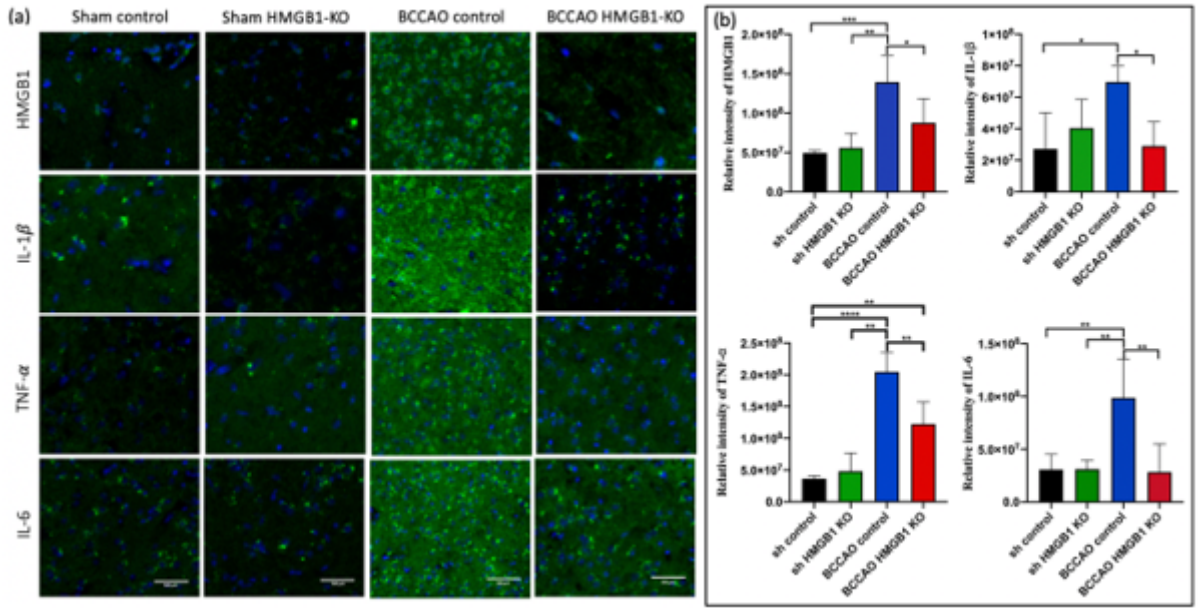

Figure 8

Decreased of HMGB1, TNF-α, IL-1β, and IL-6 expression in BCCAO HMGB1-KO mice after injection of HMG-1 CRISPR/Cas9 KO plasmid, showed by immunofluorescence (*p<0.05; **p<0.01; ***p<0.001); scale bar=100 μm

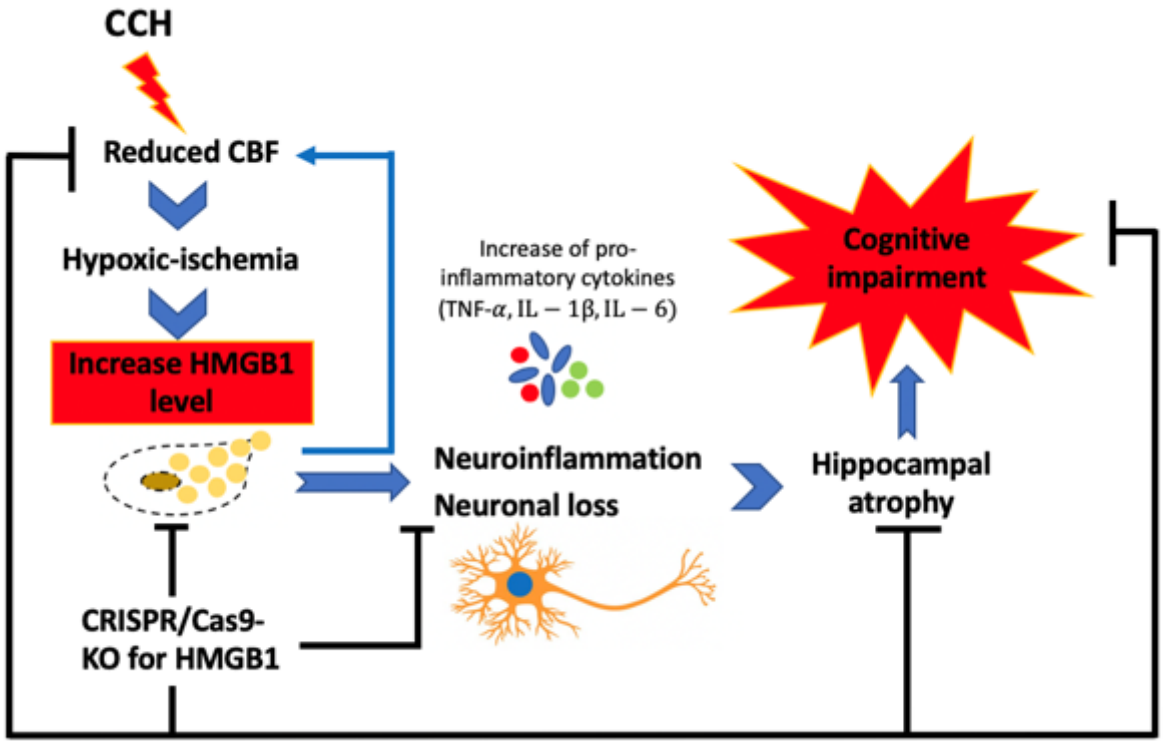

Figure 9

Summary of the study (CCH=chronic cerebral hypoperfusion, CBF=cerebral blood flow; KO=knock-out)